ACTA CHEMICA IASI, **34_2**, 295-336 (2026)
DOI: 10.47743/achi-2026-2-0013

Article

PREPARATION AND CARACTERISATION OF LOW DENSITY POLYETHYLENE/MONTMORILLONITE NANOCOMPOSITES PREPARED *VIA* MELT EXTRUSION FOR REMOVAL OF CRYSTAL VIOLET DYE POLLUTANT

Soufiane Boudjemaa[a,b*] and Hamoudi Mekhalfi[a,b]

[a]*Laboratory of Chemical Process Engineering, University Ferhat Abbas of Setif-1, Algeria*

[b]*Department of Material Sciences, Faculty of Science and Technology,University Mohamed El Bachir El Ibrahimi of Bordj Bou Arreridj, Algeria*

Abstract: In this work, the effect of montmorillonite (MMT) nanoclay on the structure, morphology, thermal, mechanical, and barrier properties of the resulting low density polyethylene (LDPE) nanocomposites prepared via melt extrusion was investigated and then used for the removal of crystal violet (CV) dye from contaminated water. In the XRD results, the observation of small pick shoulders (d_{001}) and almost no reflection in the X-ray diffractrograms indicated, respectively, the establishment of intercalated/exfoliated structures and major exfoliation of MMT clay into polymer. This observation was supported by TEM microscopy. TGA results revealed improved thermal properties in comparison with the pure polymer. DSC analysis indicated that increasing clay content above 3 wt.% effectively reduces the crystallinity of LDPE/MMT nanocomposites . The tensile strength of LDPE increased gradually with an increased content of MMT nanoclay. As the content of MMT nanoclay was increased to 10 wt.%, the permeability of the nanocomposite films to oxygen and water vapor notably

* Soufiane Boudjemaa, *e-mail*: boudjemaasoufiane@yahoo.fr

decreased. The isothermal data obtained using batch adsorption technique were fitted using Langmuir and Freundlich equations and it was found that the experimental data is well described by the Langmuir isotherm model with a very high adsorption capacity of 746.27 $mg \cdot g^{-1}$. The kinetics of the adsorption process showed rapid dynamics and conformed to pseudo-second-order model with a correlation coefficient of $R^2 > 0.99$. The influence of interaction time and initial dye concentration on the adsorption efficiency were also investigated. Additionally, thermodynamic studies revealed that the adsorption process was spontaneous and endothermic. Further, the results indicated that the synthesised nanocomposites adsorb crystal violet dye efficiently (≈ 96%) with a small decrease in removal efficiency even after five cycles of adsorption and could be employed in wastewater treatment for the removal of cationic dyes

***Keywords*:** clay/polymers nanocomposites; thermal and mechanical properties; barrier property; wastewater treatment; thermodynamic study; adsorption kinetics; crystal violet dye.

Introduction

Clay-polymer nanocomposites have received great attention in recent years due to their exceptional properties, such as increased thermal stability, high fire resistance, and enhanced mechanical characteristics, compared with traditional polymer composites.[1,2] The improvement of many properties of clay-polymer nanocomposites could be achieved using a relatively low clay loading (usually < 10 wt %) in a polymer matrix.[3] The performance of nanocomposites depends on their features such as their size, aspect ratio, surface area, volume fraction and also their compatibility with the other types of matrix. Nanocomposites have been extensively investigated to enhance their mechanical properties, improve thermal stability and sensitivity, gas barrier performance and reduce flammability to be used in various applications at low filler loading. The types of clay filler play an important role in developing better properties.[4,5]

Among the layered silicates, montmorillonite (MMT) is one of the most widely utilized silicates to fabricate clay-polymer nanocomposite,

mainly because MMT is easily available with a high aspect ratio and high expansion capacity.[6] The unit crystal structure of MMT consists of two silicon tetrahedral sheets and a central sheet of alumina octahedrons.[7] The negative charge is generated on the surfaces of the MMT layers due to the isomorphic substitutions of lower valence ions (Mg^{2+}, Fe^{2+}) for the central atoms (Al^{3+}, Si^{4+}) in the interior crystal layers of the MMT.[8] To neutralize the negative charges, hydrated cations (Na^{+}, Ca^{2+}) are electrostatically adsorbed inside the interlayer space and on the surface of MMT.[9]

Among the commodity plastics used in the packaging industries, low density polyethylene (LDPE) is the simplest and the most widely used for food packaging applications with various formats, i.e., films, sheets, bottles, cups, tubes, and trays[10,11] due to the good heat-sealability, chemical inertness, and safety of LDPE as a food contact material. Conventional LDPE is a good moisture barrier, but has a low tensile strength and has poor gas barrier properties against oxygen and carbon dioxide.[12, 13] Various efforts have been made to improve the fundamental properties of LDPE for use in active food packaging as an advanced functional material. A large number of hybrid systems have been investigated by blending organic or inorganic particles (i.e. silica, calcium carbonate, graphene, silver nanoparticles, etc.) into a LDPE matrix to enhance the modulus strength and gas barrier properties.[14, 15]

The first objective of this work was to study the influence of exfoliated MMT nanoclay incorporated into LDPE and, in particular, the effect of different amounts of MMT (0.5–10%) on the morphological, thermal, mechanical and barrier characteristics of the formed LDPE/MMT nanocomposites. The crystallinity and the MMT nanoclay distribution in the LDPE matrix were also to be examined.

In the other hand, it is known that the industry is a major cause of water pollution because of the important volumes of extensively contaminated wastewater that it discharges into the environment.[16] The dyes are among of hazardous chemical compounds presented in the textile effluent which are toxic to aquatic and non-aquatic organisms and can cause cancer for humans.[17] As a result, the direct discharge of effluent into water causes ecosystem and health problems.[18] These hazardous organic compounds also affect the aquatic life by altering the photosynthetic activity of the biota due to reduced light penetration through water.[19] Crystal violet (CV) is one such and common type of dye extensively used by the paper and textile industry. It is also used as a biological stain and dermatological agent in human and veterinary medicine.[20] In spite of its wide use, CV dye has been found to have harmful effects on humans and has been suspected to be a potential carcinogen. Consumption of the dye even in small amount (<1ppm) may result in respiratory disorders, kidney failure and permanent blindness. Its exposure to large amounts irritates the skin and the digestive tract.[21] Belonging to the class of triarylmethane dyes, it has a complex chemical structure and long half-life which results in their persistence in the environment for a very long time, aggravating the problem further.[22] The dye has also been found to be teratogenic and mutagenic and is thus, categorized under biohazards.[23] Therefore, an increased interest has been focused on removing such dyes from the industrial wastewater prior to its reuse or discharge into the aquatic environment.

Given the environmental effect caused by dye pollution, effective methods should be used to treat wastewater polluted by coloring agents, such as CV dye, before their release into the environment. Among several physical and chemical techniques used to removal of CV dye effluents such

as coagulation–flocculation,[24] electrocoagulation,[25] photocatalysis,[26] membrane filtration,[27] and several other techniques, adsorption techniques are widely used due to their simplicity,[28] low cost and ease of process. To remove dyes from aqueous environments, many different types of adsorbents have been used, including activated carbon,[29] agricultural and industrial wastes, biosorbents,[30] clays[28] and clay-polymer nanocomposites.[31] Our study lies in utilizing LDPE /Algerian montmorillonite as an eco-friendly and cost-efficient adsorbent for the removal of the CV dye from aqueous solutions. Moreover, we investigate the reusability of the nanocomposite adsorbent to further minimize the cost of treating polluted water. This comprehensive exploration aims to contribute to both the advancement of polymer nanocomposites and the effective treatment of wastewater contaminated with CV, addressing critical environmental and health concerns.

Experimental

Materials

The polymer matrix used in this study was a linear low-density polyethylene grafted with maleic anhydride, trade name LF-Y819-A, from NOVA Chemicals Novapol (China). The density and the melt flow index (MFI) are, 0.92 g/cm^3 and 0.75 g/10 min, respectively (190 °C/2.16 kg) while the maleic anhydride (MA) content is 1 wt%. Natural montmorillonite (MMT) was supplied by the County of Maghnia, Western Algeria, and used after purification. The Crystal violet (CV) dye was purchased from Sigma Aldrich, with a molecular weight of 407.99 g.mol^{-1} and solubility in water of 4g.L^{-1}, and its chemical structure is depicted in Figure 1.

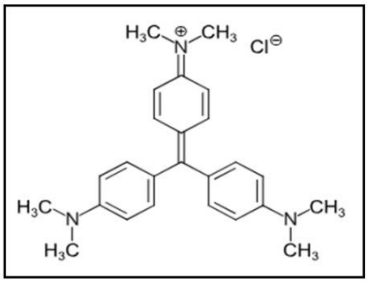


Figure 1. Chemical structure of the Crystal violet (CV) dye (Chemical formula: $C_{25}H_{30}ClN_3$).

Montmorillonite pre-treatment

50 g of montmorillonite (MMT) clay was placed in a 750-mL vessel containing distilled water and stirred for 2 h. The suspension was decanted and separated by centrifugation. This procedure was repeated four times. Finally, the precipitate (MMT) was oven dried at 120 °C for 24 h and crushed. The chemical composition of of the dried samples is given in Table 1.

Table 1. Chemical composition (wt %) of initial MMT according to XRF analysis.

Compound	SiO_2	Al_2O_3	Fe_2O_3	TiO_2	P_2O_5	SO_3	K_2O	MnO	ZrO_2	CaO
Weight %	71.60	12.75	10.77	1.66	0.70	0.09	0.09	0.02	0.04	0.31

Preparation of LDPE/MMT nanocomposite

Nanocomposites LDPE/%MMT were prepared by melt extrusion to yield composite film samples with MMT nanoclay contents of 0.5, 1, 3, 5, and 10 wt%. Nanocomposites were prepared using a corotating twin-screw extruder (Haake Polylab Rheomex OS PTW16, D = 16 mm, L/D = 40) coupled with a Haake Metering Feeder to control the feed rate. The LDPE and MMT nanoclay masterbatch pellets were dried in a convection oven at 80 ºC for 24 h and mixed in a sealed plastic bag by manual tumbling prior to being fed into the extruder. The temperature profile used in this study was 170–180 °C from hopper to die, the feed rate was fixed at 1 kg/hr, and the

screw speed was set at 180 rpm. All materials were manually premixed before introduction into the twin-screw extruder. The pellets that were obtained after extrusion were press-molded using an electrically heated hydraulic press to form films of thickness 50 mm in order to facilitate evaluation of the physical properties. The molding temperature and pressure were 175 °C and 4 MPa, respectively. Neat LDPE films were prepared under the same conditions to get a reference material. The measured surface physical characteristics of the prepared LDPE/5%MMT nanocomposite are illustrated in Table 2. A high specific surface area and negatively charged surface in the Table 2 suggests the suitability of the nanocomposite to adsorb cationic dyes.

Table 2. Surface physical characteristics of the LDPE/5%MMT nanocomposite.

Parameter	Value
BET surface area (m2 g^{-1})	242.1
Total pore volume (cm3 g^{-1})	5.652
Average pore size (nm)	0.342
Zeta potential (mV) Ph = 6.2	−25.90

Adsorption of Crystal Violet dye experiments

In the present series of experiments, the influence of dye concentration (50–200 mg L^{-1}) and contact time on the adsorption of CV were studied. The pH of the dye solution was maintained at 6.2 in all the measurements. In each adsorption experiment, 25 mg of LDPE/5%MMT nanocomposite adsorbent was added to 100 mL samples of the dye solution with known concentration and the mixture was stirred in a thermostatic water bath oscillator at 313 K for pre-determined time interval at 130 rpm agitation speed. To observe the effect of temperature, the experiments were carried out at three different temperatures, i.e. 303

K, 313 K and 323 K. During each run, aliquots of 1 mL were withdrawn from the solutions at regular intervals of time, diluted, and centrifuged for 10 min at 8000 rpm to measure absorbance of the supernatant solution. The concentration of the CV dye in the solution was measured spectrophotometrically using Lambda 950, Perkin-Elmer UV–Visible spectrophotometer (UV–Vis.) at 590 nm (λ_{max} for CV). The equilibrium amount of adsorption (q_e), the amount of adsorption (q_t) at any given time t, were computed from the following equations:

$$q_e = \frac{(C_0 - C_e)}{m} \times V \quad (1)$$

$$q_t = \frac{(C_0 - C_t)}{m} \times V \quad (2)$$

And, the dye removal efficiency was calculated using the following equation:

$$\text{Removal efficiency}(\%) = \left(\frac{C_0 - C_t}{C_e}\right) \times 100\% \quad (3)$$

where C_o (mg·L^{-1}), C_e (mg·L^{-1}), and C_t (mg·L^{-1}) correspond to the dye concentrations at the initial, equilibrium and time t (min), V (L) is the volume of the solution, and m (g) is the weight of the adsorbent.

Characterization

X-ray diffraction (XRD) measurements were carried out using a Philips diffractometer (PW-1710). Using a CuKα (λ = 1.54 Å) radiation at 40 KV and 30 mA, all scans were performed in 2θ range at 4 – 75° with a scan speed of 2 deg/min.

The morphology of the samples surfaces were investigated using scanning electron microscopy (SEM) (JSM-5900 LV).

Chemical analysis was performed by X-ray fluorescence (XRF) spectroscopy on ElvaX Pro (Elvatech) spectrometer.

Fourier transform infrared (FTIR) spectra of MMT were recorded with the Fourier Spectrophotometer Spectrum type Shimadzu FTIR-8300 in the range of 400-4000 cm^{-1}, using KBr disc method. The morphology of MMT was analyzed by a scanning electron microscope (SEM) (JSM-5900 LV).

The specific surface area (SSA) and cation exchange capacity of the MMT sample were determined by methylene blue titration and spot methods, respectively.[32]

Thermal gravimetric analysis (TGA) was conducted on a Shimadzu TGA- 51H analyser with temperature program = heat from 30 °C to 900 °C; heating rate of 10°C / min in Nitrogen atmosphere with a purge rate of 20 mL/min.

The differential scanning calorimetry (DSC) analysis was conducted on a Shimadzu DSC-60 calorimeter with N_2 as a purge gas, with a heating rate of 10°C/ min.

Bright field transmission electron microscopy (TEM) images of the nanocomposites were obtained at 80 kV, with a Zeiss EM 900. The samples were cooled at -80°C and then microtomed with a diamond knife cooled at -60 °C to give sections with a nominal thickness of 50 mm and 1 mm^2 of superficial area. The sections were collected on the surface of a solution of dimethylsulphoxide/water, 60/40 parts, respectively, and then transferred on Cu grids of 200 mesh.

The oxygen transmission rates (OTR) of the LDPE/MMT nanocomposite films were measured using an OTR 8001 oxygen permeation analyzer (Systech Instruments Co. Ltd., Johnsburg, Illinois, USA) at 23 ºC and 0% RH according to the ASTM D3985 method.

The water vapor transmission rate (WVTR) was determined using a WVTR 7001 water vapor permeation analyzer (Systech Instruments Co. Ltd., Johnsburg, Illinois, USA) at 38 ºC and 95% RH according to the ASTM F1249 method.

Results and discussion

1. Characterization of MMT nanoclay

1.1. Scanning electron microscope (SEM) analysis

SEM analysis is another important tool used in the determination of the surface morphology of MMT. SEM micrograph of the MMT sample suggests that it is a very cohesive material (Figure 2). The micrograph confirms that the material forms micron-size agglomerates. A higher magnification micrograph of the same structure shows that the micro-size particles are composed of individual platelets, which conglomerate into larger size particles.

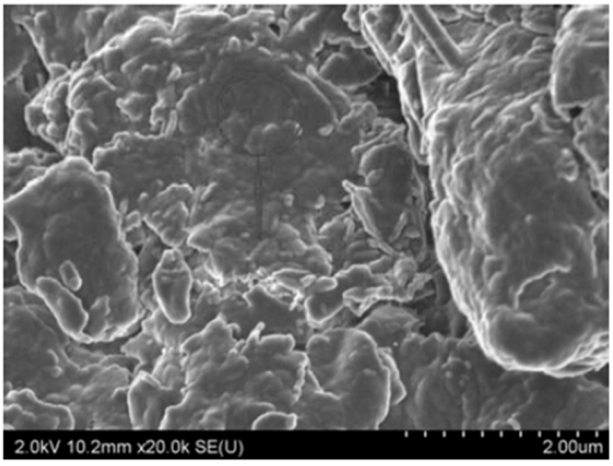


Figure 2. SEM micrograph of MMT.

1.2. IR spectroscopy

FT-IR spectra provide useful information about the surface functional groups which to a great extent affects the adsorption process of contaminants to an adsorbent surface. For this reason, the FT-IR spectrum of the MMT clay was recorded as shown in Figure 3. As noted, all the spectra show bands at 3636 and 3395 cm^{-1} attributed to O–H stretching for the silicate and water, respectively, 1631 cm^{-1} (related to O–H bending), 1039 cm^{-1} (owing to stretching vibration of Si–O–Si from silicate), 912

cm^{-1} (from Al–OH deformation of aluminates), 525 and 470 cm^{-1} (Al-O stretching and Si-O bending vibrations of MMT, respectively), and 789 cm^{-1} (related to Si-O stretching vibration).[33]

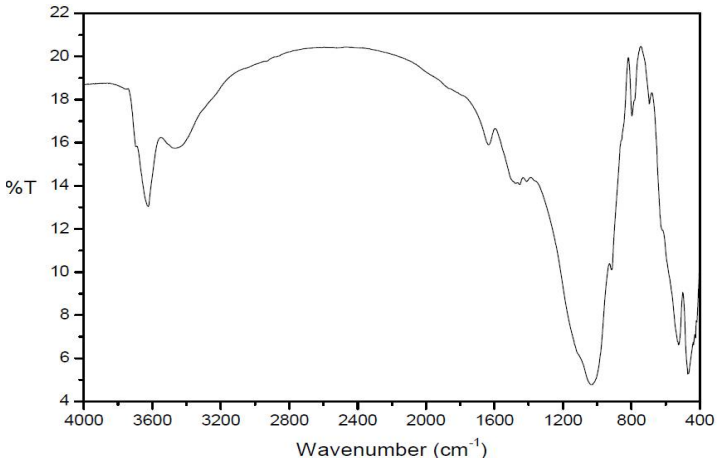


Figure 3. FTIR spectrum of MMT.

1.3. XRD analysis

XRD analysis is widely used to investigate the mineralogical composition of clay minerals which deeply affects their physiochemical properties. For this purpose, the MMT powder sample was subjected to XRD analysis and the result is shown in Figure 4. The X-ray diffraction pattern of MMT shows the major phase of montmorillonite whose main peak is at 2θ = 19°, 22°, 28°, 37° and 53°. The presence of Quartz at 2θ = 23° and 29° was noted. A peak of 2θ = 34° appears on the sample with a different intensity, which can be attributed, presumably, to calcite. The reflection at 2θ = 32° on the MMT clay proves the presence of sodium feldspar.[34,8]

Bragg's equation, $2d\sin\theta = n\lambda$, was used to calculate the basal spacing (d_{001}) of the MMT. The characteristic d_{001} diffraction peak for MMT in the 2θ region is located at 6.52°, d_{001} = 13.54 Å[35].

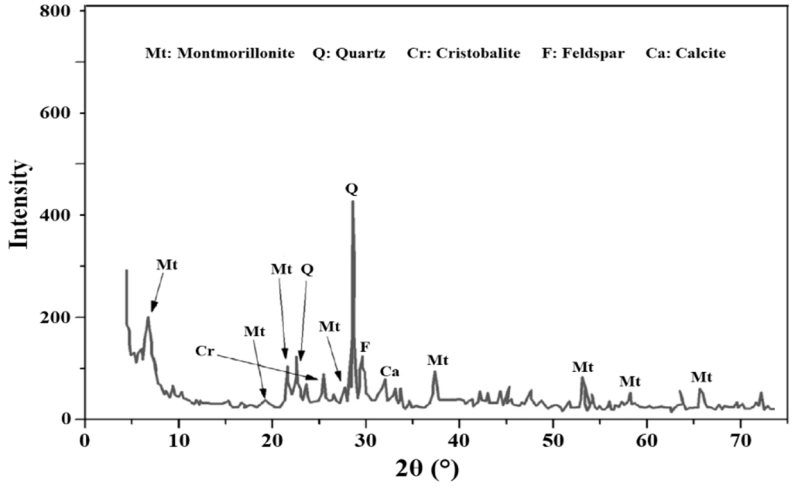


Figure 4. XRD pattern of MMT.

1.4. Specific surface area (SSA) and cation exchange capacity (CEC)

Surface area and cation exchange capacity measurements of clay minerals are important for characterizing their bonding and swelling power, adsorptivity for polar compounds, and plasticity. Methylene blue (MB) spot and titration methods are widely used for SSA and CEC determination where they estimate them more accurately than other conventional methods. Equations (1) and (2) are used to calculate SSA and CEC[32], respectively:

$$SSA = \frac{m_{MB}}{319.87} \times A_V \times A_{MB} \times \frac{1}{m_s} \quad (4)$$

$$CEC = \frac{100}{m_s} \times V_{cc} \times N_{mb} \quad (5)$$

where m_{MB} is the mass of the adsorbed MB at the point of complete replacement, m_S is the mass of the clay specimen, 319.87 is the molecular weight of MB dye, A_V is Avogadro's number (6.023×10^{23}/mol), A_{MB} is the area covered by one MB molecule, V_{CC} is the volume of the MB titrant, and N_{mb} is the normality of the MB (meq/mL). By substitution in Equations (1) and (2), it was found that the SSA and CEC of the MMT are 177m^2/g and

94 meq/100g, respectively. For comparison purposes, SSA was also measured by N_2 adsorption method (Brunauer–Emmett–Teller: BET specific surface area) using a Quantachrome Monosorb®device (Quantachrome Instruments, Boynton Beach, Florida, USA) and it was found to be 75.5 m^2/g. This value is very small compared to that estimated by MB test because the N_2 adsorption method (BET) estimates the external surface area rather than total surface area for swelling silicates.

1.5. Thermogravimetric analysis (TGA)

The TGA and DTGA curves for MMT are shown in Figure 5.

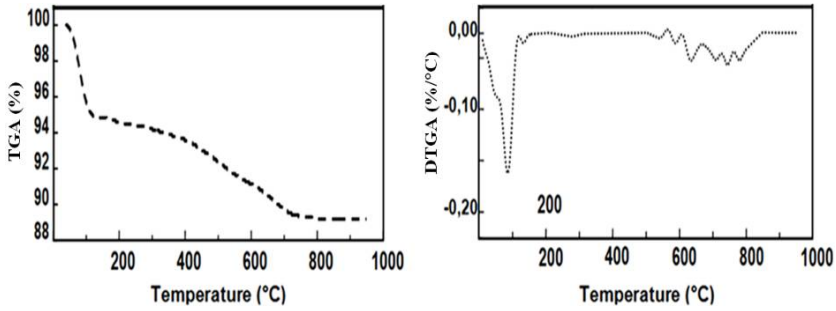


Figure 5. TGA and DTGA curves of MMT.

MMT displays two thermal degradation transitions. The first one occurs in the temperature range 100–350 °C and is due to the vaporization of both the free water (i.e., the water sorbed on the external surfaces of crystals) and the water residing inside the interlayer space, forming hydration spheres around the exchangeable cation.[8] The second transition takes place at higher temperatures (between 500 and 800 °C) owing to the structural water resulting from the dehydroxylation of clay OH units.

2. Nanocomposites LDPE/MMT characterization

2.1. IR spectroscopy

The FTIR spectrum of LDPE and LDPE/MMT nanocomposites is presented in Figure 6.

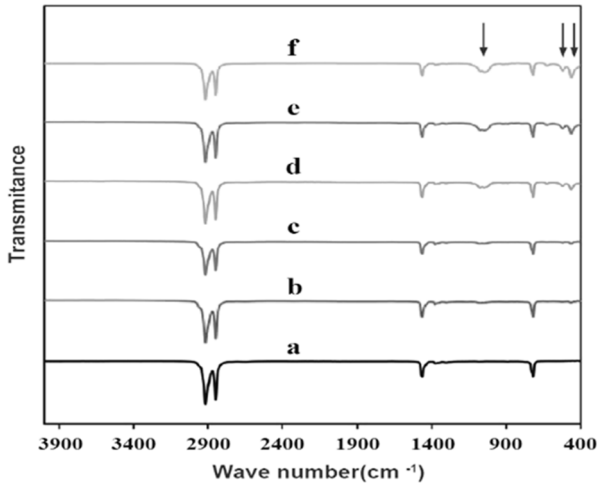


Figure 6. FTIR spectra of LDPE /MMT nanocomposites with different MMT contents: (a) 0, (b) 0.5, (c) 1, (d) 3, (e) 5 and (f) 10 wt%.

FTIR is widely used for the identification of specific chemical groups in materials. Clear additional absorption peaks were identified at about 464, 521, and 1047 cm^{-1} in the FTIR spectra of LDPE/MMT nanocomposites films. These values correspond to IR absorption peaks typical for silica and alumina and most likely originated from the stretching and bending.[36] The peaks characteristic of the MMT nanoclay became more intense as the content of MMT nanoclay in the composite system was increased.

2.2. XRD analysis

XRD is a most useful technique for the measurement of d-spacing of ordered intercalated and exfoliated nanocomposites. XRD patterns exhibit the formation of intercalated or semi exfoliated composites with the help of movement of the diffraction peak while the disappearances of this diffraction peak indicate possible exfoliation of clay platelets in the polymer matrix.[37] Figure 7 illustrates the XRD patterns of LDPE/MMT nanocomposites at different concentrations of clay content. For LDPE, the

presence of two crystalline peaks at 21° and 23.3°, related to the (110) and (200) planes, respectively, characteristic of the orthorhombic structure of the crystal polyethylene was observed.[38,39,4] For LDPE/MMT significant increase in the intensities of the 6 and 18º 2θ diffraction peaks was observed for samples with 0.5 wt % nanoclay. These peaks were assigned to the (001) and (020) planes of the clay-stacked layer structure and agreed with values reported by Zbik *et al.*[40] and Merinska *et al.*[41] At low volume fractions of the MMT nanoclay, these diffraction peaks appeared as very weak shoulders. As the content of MMT nanoclay was increased, however, the same peaks became significantly more pronounced. As shown in the Figure 7, the presence of an intercalated/exfoliated morphology, combined with the high interfacial area and adhesion between the polymer and the clay, hinders PE chain mobility, with two effects: a reduction in the crystallinity degree (related to the peak intensity) and dimension of the crystallites (related to the peak broadening and shift).[42]

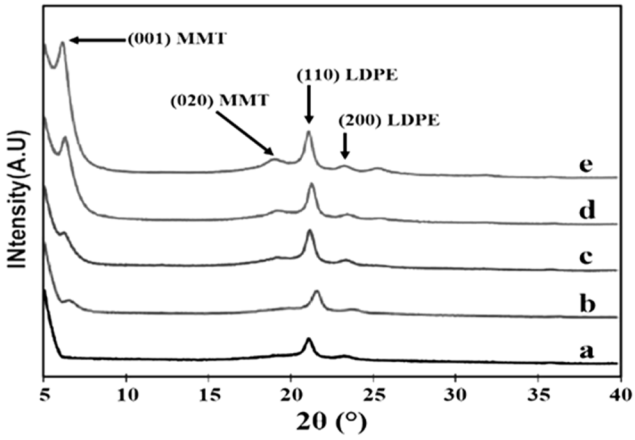


Figure 7. XRD patterns of LDPE /MMT nanocomposites with different MMT contents: (a) 0, (b) 0.5, (c) 1, (d) 3 and (e) 5 wt%.

2.3. TEM

The MMT nanoclay particles dispersed in the LDPE matrix can be readily identified using TEM as dark lines in the LDPE/MMT

nanocomposite film that was prepared using 5 wt% MMT (Figure 8a). The TEM analysis revealed that a large proportion of the clay layers was in the exfoliated state. Kim *et al.*[43] reported that the shear force exerted during the extrusion process promoted nanoparticle dispersion by partially disrupting the stacking order of clay layers, while the molten polymer can at the same time enter and penetrate the MMT nanoclay interlayers. Close examination of some platelets (highlighted with white arrows in Figure 8.b, white grayscale), however, revealed the presence of stacked structures, which suggests that some intercalated features in the LDPE matrix remain. Abbasian *et al.*[44] explained that the shear force exerted by the extrusion process is not always sufficiently high to achieve complete break-up of large agglomerates, which thereby allows clusters of nanoparticles to persist. Put together, these results indicate that the clay layers in LDPE/MMT nanocomposite films were present in a mixed form and mostly consisted of well dispersed exfoliated layers with a small amount of intercalated MMT nanoclays.

Close examination of some platelets (highlighted with white arrows in Figure 8b, white grayscale), however, revealed the presence of stacked structures, which suggests that some intercalated features in the LDPE matrix remain. Abbasian *et al.*[44] explained that the shear force exerted by the extrusion process is not always sufficiently high to achieve complete break-up of large agglomerates, which thereby allows clusters of nanoparticles to persist. Put together, these results indicate that the clay layers in LDPE/MMT nanocomposite films were present in a mixed form and mostly consisted of well dispersed exfoliated layers with a small amount of intercalated MMT nanoclays.

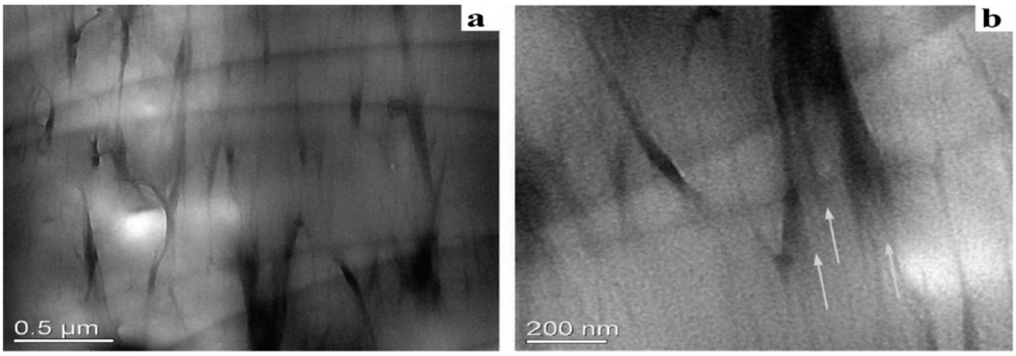


Figure 8. TEM Micrograph of LDPE/5% MMT nanocomposite with different scales: (a) 0.5 µm and (b) 200 nm. Indicate the presence of intercalated MMT nanoclays in the LDPE.

2.4. Thermal properties

The thermal degradation behavior of a polymer in terms of weight loss as a function of temperature is typically determined using TGA. The important parameters in such analyses are the degradation onset temperature ($T_{10\%}$, determined as the point at which 10% of the sample weight has been lost) and the degradation mid-point ($T_{50\%}$).[45,4] In the present study, the thermal stability of nanocomposites was generally higher in comparison to the pristine LDPE (Table 3). The temperature marking the onset of thermal degradation ($T_{10\%}$) was significantly higher in the nanocomposites than that determined for LDPE (436 ºC). The $T_{50\%}$ value of the nanocomposites was also found to increase with increasing MMT nanoclay content and the maximum $T_{50\%}$ value of 497 ºC was determined at 10 wt% MMT nanoclay loading. These results are in agreement with those reported in other studies.[46] These improvements in thermal stability can be explained by the formation of an insulating and incombustible multilayered carbonaceous-silicate char on the composite surface during combustion. This char can obstruct the escape and diffusion of low molecular weight volatile products within the nanocomposites, while simultaneously insulating the polymer underneath the char layer from surrounding heat.[47] The physical-chemical

adsorption of volatile decomposition products on silicates/clays, additionally, can delay the volatilization of products that are generated from carbon-carbon bond scission within the LDPE matrix.[48]

The thermal properties of LDPE/MMT nanoclay composites, such as melting temperature, fusion enthalpy, and degree of crystallinity for non-isothermal crystallization, were also studied using DSC. The degree of crystallinity (X_C) was calculated according to the following equation:

$$X_C = \frac{\Delta H_m}{\Delta H_m^0} \times 100 \qquad (6)$$

where ΔH_m is the experimental heat of fusion (J/g) and ΔH_m^0 is the theoretical heat of fusion of 100% crystalline LDPE (293J/g). The melting temperature (T_m) and the heat of fusion were determined during the second round of heating and are shown for each sample in Table 3.

Table 3. Melting temperature, melting enthalpy, and crystallinity values for 10% and 50% weight loss for LDPE/MMT nanocomposite films with various MMT contents (wt%).

Sample	$T_{10\%}$ (ºC)	$T_{50\%}$ (ºC)	T_m (ºC)	Melting Enthalpy (J/g)	Crystallinity (%)
LDPE	436	475	107.08	161.1	54.08
LDPE/0.5 %MMT	450	484	105.87	170.0	58.02
LDPE/1 %MMT	450	486	105.98	179.0	61.09
LDPE/3 %MMT	461	491	106.42	180.5	61.60
LDPE/5 %MMT	464	493	106.11	162.0	55.29
LDPE/10 %MMT	465	497	106.21	161.9	55.26

$T_{10\%}$: Temperature at 10% weight loss (ºC) ; $T_{50\%}$: Temperature at 50% weight loss (ºC).

The DSC analysis showed that the melting temperature (Tm) decreased slightly as the MMT nanoclay content was increased. This change can be attributed to the differences in crystal properties (e.g., crystal type, packing density, crystallite size, and distribution) between the

nanocomposites and pristine LDPE.[49] A study by Jayrajsinh *et al.*[50] revealed that layers of MMT nanoclay can act as nucleating agents that facilitate crystal growth by providing a higher level of nucleation density. This process may involve crystal formation and accounts for the changes in Tm. In addition, an increase in the clay mineral content to 3 wt.% increased significantly both the melting enthalpy and crystallinity. Specifically, a 12% increase in crystallinity for the nanocomposites was observed, which suggests that the filler in the LDPE matrix played a role in nucleation processes.[51] Jayrajsinh *et al.*[49] reported that the crystallinity of LDPE/PE-g-MA/clay composite (where PE-g-MA represents polyethylene grafted maleic anhydride) increased with an increased content of organomontmorillonite and that the maximum of crystallinity was found at 3 wt.% clay mineral content. The authors additionally found that the level of crystallinity decreased with a further increase in clay mineral content. This observation is in agreement with the present results, which showed that the degree of crystallinity decreased when the MMT nanoclay concentration was increased above 3 wt %. Particularly, this behavior arose because the perfection of the crystals was affected by the restricted mobility of LDPE chain segments, which consequently slowed down the growth of well-developed lamellar crystals. This restriction increased with an increased content of MMT nanoclay and, thereby, yielded less perfect crystals. The combined influences of excess nucleation sites and retarded crystal growth led to the production of fine crystals, which, in turn, resulted in a lower degree of crystallinity.[52]

2.5. Mechanical properties

The tensile strength and elongation were examined as a function of clay mineral content (Figure 9). The results revealed that the tensile strength in the machine direction increased significantly from 11.99 N/mm^2 to 16.89 N/mm^2 as the MMT content was increased from 0 to 10 wt %. This

result revealed two possible explanations for the increase in tensile strength in the prepared LDPE/MMT nanocomposites.[53] The first explanation may stem from an increase in crystallinity as was observed in the DSC analyses. The greater the crystallinity, the greater the energy absorbed and the greater the modulus.[54] Although the mechanical properties of a nanocomposite are related to the crystallinity of the polymer matrix, Shebani *et al.*[55] observed that the behavior of the composite was not simply a function of crystallinity and crystal structure (morphology), but was instead a complex function that involved additional factors, such as lamellar thickness and interfacia interactions. A comprehensive study by Hussein *et al.*[56] showed that a filler with an aspect ratio greater than 20 – 30 can be considered as an effective reinforcement filler and yields a nanocomposite with apparently increased stiffness. The proposal from the present study was, therefore, that the improved tensile strength can be attributed to the high specific surface area (750 – 800 m^2/g) and large aspect ratio (50-1000) of the well dispersed MMT clay within the LDPE matrix.[53] Similarly, previous work has shown that the dispersion of nano-scale silicate layers in a polyolefin matrix led to an improvement in mechanical strength.[54] The stiffness of MMT nanoclay plates hindered the mobility of polymer phases and prevented the slippage of polymer chains past one another. The stiffness also retarded the plastic deformation and, thereby, resulted in stretching resistance and lower elongation.[55] This description was supported by the decreased elongation of LDPE/MMT nanocomposites as a function of increased clay mineral content (Figure 9). The elongation dropped significantly from 592.28% for pristine LDPE to about 323.50 % for the LDPE-MMT with 10 wt.% clay mineral content. Fu and Naguib[57] proposed that this reduction stemmed from the weak interactions between the polymer matrix and fillers as well as from the formation of agglomerated nanoclay, which created stress

concentrations in the polymer matrix. LDPE, therefore, lost its plastic properties as a result of the increased stiffness value.

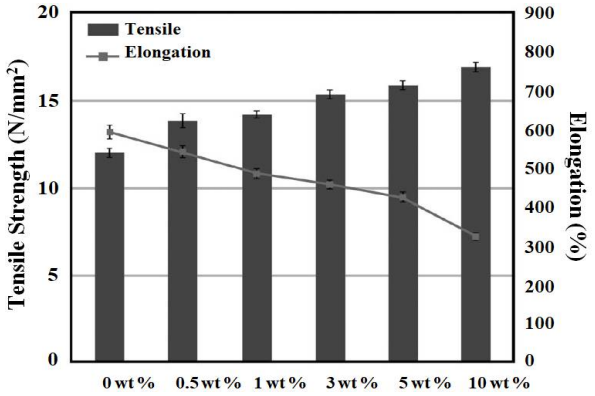


Figure 9. Tensile strength and elongation of LDPE/%MMT nanocomposites films using different MMT contents (wt %).

2.6. Barrier properties

The LDPE/MMT nanocomposites showed similar trends in behavior for both the oxygen and water vapor permeability (Figure 10). The permeability was found to decrease gradually as the concentration of clay mineral increased from 0.5 wt.% to 10 wt.%. Specifically, oxygen permeability decreased from 306 to 175 mL mm/m^2 day atm (42.8% reduction) while the water vapor permeability decreased from 0.600 to 0.443 g mm/m^2 day atm (26.2% reduction). These changes most likely arose as a result of the high aspect ratio of exfoliated and intercalated clay platelets in the LDPE matrix. In particular, as shown in Figure 8, when the layers are aligned in the direction parallel to the film surface, the resulting tortuous path delays diffusion of both gas and water vapour.[58]

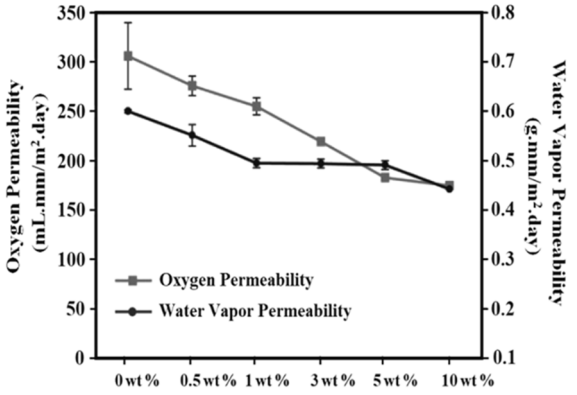


Figure 10. Oxygen and water-vapor permeability values of LDPE/ MMT nanocomposites films using different MMT contents (wt %).

2.7. pH at point zero charge

The zero charges point (pHpzc) is a critical parameter which indicates a pH-value where the surface charge on the adsorbent has a zero charge. Thereby, the surface charge of solid is negative if pH > pHpzc and positive if pH < pHpzc.

The pH of suspension of the selected sample for adsorption (0.15 g of LDPE /5%MMT,) and NaCl aqueous solution (50 mL, 0.01 mol L^{-1}) was adjusted to initial values ranging from 2 to 12. The suspensions were agitated 48 h at room temperature, and the variation of pH (ΔpH = pHfinal − pHinitial) was measured and plotted versus the initial pH. The pHPZC is identified as the point at which the variation of pH is equal to 0, as shown in Figure 11. The pHpzc of nanocomposite was found to be at a pH = 6.8.

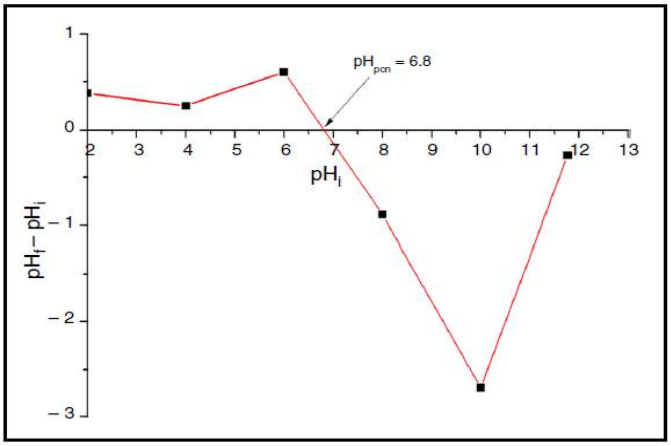


Figure 11. Isoelectric point (pHpcn) determination for LDPE /5%MMT nanocomposite.

3. Adsorption studies

3.1. Effect of pH

The surface charge of the adsorbent can be affected by the pH of the solution, which creates the essential force between the adsorbent and the adsorbate.[59] Figure 12 shows the pH effect on the adsorption of the CV dye onto LDPE/5%MMT nanocomposite sample. As can be seen from figure, the adsorption capacity remains stable throughout the pH range (2 – 12) indicating that the adsorption is independent of pH.

The similar results were reported by Kırans et al.[60] for studying the adsorption of an anionic dye onto clay. Hence, we conclude that the pH has no effect on the adsorption capacity of LDPE/5%MMT nanocomposite. This behaviour was explained by electrostatic interactions between the negative charges of the Cl^- group of the dye and the positive charges of MMT of the nanocomposite adsorbent.[58]

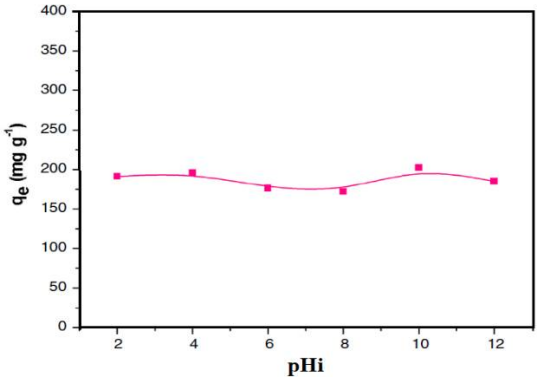


Figure 12. Effect of pH on adsorption of CV by LDPE/5%MMT nanocomposite.

3.2. Effect of initial dye concentration

The plot displaying effect of initial dye concentration of CV on LDPE/5%MMT nanocomposite adsorbent surface at pH 6.2 and 30°C exhibits continuous increase in equilibrium adsorption capacity from 184.67 to 583.08 mg·g^{-1} with increasing dye concentration ranging from 50 to 200 mg·L^{-1} (Figure 13).

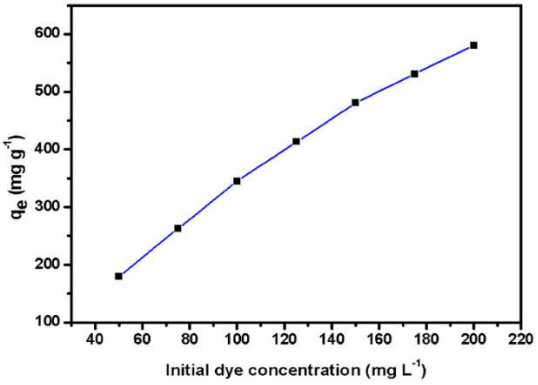


Figure13. Effect of initial dye concentration on the adsorption capacity of CV dye onto LDPE/5%MMT nanocomposite at pH 6.2 and 30 °C.

This enhanced adsorption capacity is attributed to the high concentration gradient between the dye molecules and the number of pores available for their diffusion through π-π interactions and weak hydrogen bonding at the

beginning of the adsorption process. Also, the functional groups present on the surface as well as inside the pored network may also have resulted to be a high driving force for the adsorption of CV dye molecules from solution to the surface of MMT. Hence, a higher initial concentration of the dye will assist in overcoming mass transfer resistance between the aqueous and solid phases, thereby, favouring the adsorption process.

3.3. Effect of contact time

To study the effect of reaction time on the adsorption of dye onto LDPE/5%MMT nanocomposite, the exposure time was varied between 0 and 30 min (Figure 14).

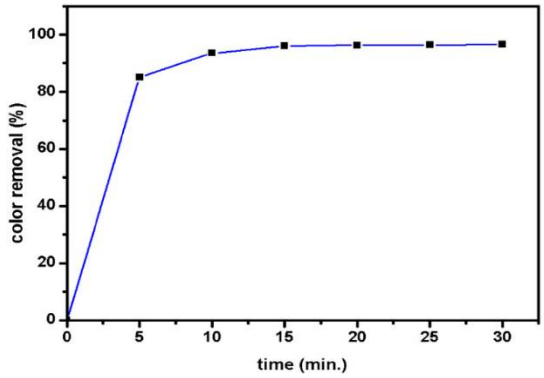


Figure 14. Effect of contact time on the adsorption capacity of CV dye onto LDPE/5%MMT nanocomposite at pH 6.2 and 30 °C.

The curve exhibits sharp increase in dye colour removal efficiency, approximately 85% in the first 5 min of reaction, after which the colour removal process markedly slowed down and completely saturated in 30 min with no further increase in the adsorption amount. The initial fast adsorption of dye molecules on LDPE/5%MMT nanocomposite surface is attributed to the higher availability of pores in the initial phase of the adsorption process with negligible interference from solute-solute interactions.

3.4. Adsorption kinetics

In order to investigate the kinetic mechanism of CV dye adsorption process on the LDPE/5%MMT nanocomposite, the pseudo-first-order and pseudo-second-order kinetic models are used to analyse the experimental results describing the adsorption data with reaction time by the following equations:

$$log(q_e - q_t) = log\ q_e - k_1 t/2.303 \qquad (7)$$

$$\frac{t}{q_t} = \frac{1}{k_2 q_e^2} + \frac{1}{q_e} t \qquad (8)$$

where q_t is the amount of dye adsorbed at time t (mg·g^{-1}), q_e is the adsorption capacity at equilibrium (mg·g^{-1}), and k_1 and k_2 are the equilibrium rate constants of pseudo-first-order (min^{-1}) and pseudosecond-order (g^{-1} mg·min) models, respectively. The values of qe and k_1 for the pseudo-first-order kinetic model are determined from the intercepts and slopes of plot of log (q_e-q_t) versus t, whereas the values of qe and k_2 for pseudo-second-order kinetics model are determined using the linear fit between the t/q_t and contact time (t).[61, 62]

The obtained linear plots of pseudo-first-order and pseudo-second-order kinetic model using above mentioned equations are shown in Figure 15, while the values of kinetic parameters k_1, k_2, qe and R^2 obtained by fitting the experimental data of CV adsorption are listed in Table 4. The correlation coefficient (R^2) fits better to the pseudo-second-order kinetic model than the pseudo-first-order kinetic model. Additionally, the results show good agreement between the experimental and the calculated qe values. All these results suggest that the experimental kinetic data for CV dye adsorption on LDPE/5%MMT nanocomposite follows pseudo-second-order model better than the pseudo-first-order model, indicating that the rate

limiting step may be chemisorption, involving valence force via sharing or exchanging electron between adsorbent and adsorbate.[63,64]

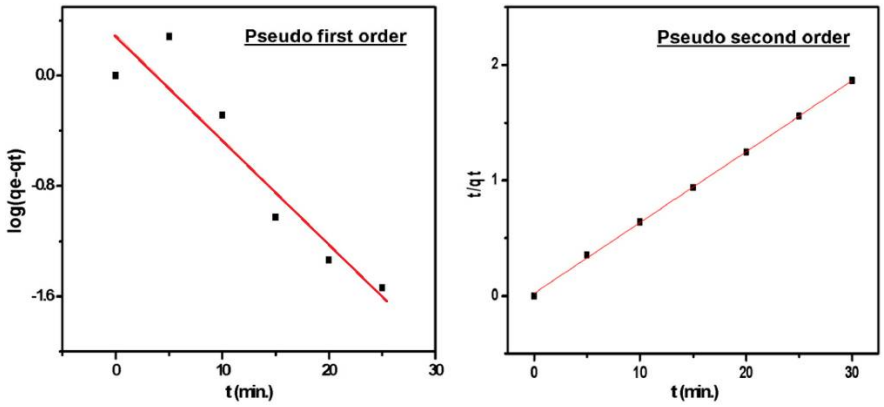


Figure 15. Kinetic plots for the adsorption of CV onto LDPE/5%MMT nanocomposite at 30 °C.

This may be attributed to the various functional groups located in LDPE/5%MMT nanocomposite due to MMT, which favours adsorption process in addition to the tetrahedral and octahedral sheets already present in the MMT In the literature, similar results have been reported where the pseudo-second-order model fitted various adsorption systems, including the adsorption of methyl green[65] and methyl blue dye[66] molecules on the montmorillonite and the adsorption of methylene blue using a novel magnetic composite bioadsorbent.[67]

Table 4. Kinetic parameters of pseudo-first-order model and pseudo-second-order model for CV dye adsorption onto LDPE/5%MMT nanocomposite.

Kinetic model	Parameters				
	k1 (min^{-1})	k2 ($g \cdot mg^{-1} min^{-1}$)	qe ($mg \cdot g^{-1}$)	R2	q_{exp} ($mg \cdot g^{-1}$)
Pseudo-first-order	0.1749	–	1.991	0.8647	16.13
Pseudo-second-order	–	0.1811	16.289	0.9994	

3.5. Adsorption isotherms

The adsorption isotherm represents systems where the adsorption process reaches an equilibrium state to reveal the interaction between the adsorbent and the adsorbate. Langmuir and Freundlich adsorption isotherm models are two generally used models to determine the mechanistic parameters associated with adsorption processes. The analysis of experimental results is done by correlating the equilibrium data with the theoretically derived equations obtained using these isotherm models. The Freundlich model uses the exponential distribution of adsorption sites and energies in an adsorption process with an assumption that the adsorbent surface sites are heterogeneously distributed and is represented by the following equation:[68]

$$log\ q_e = log\ K_F + \frac{1}{n_F} log\ C_e \qquad (9)$$

where q_e is the solid-phase equilibrium concentration (mg/g), *Ce* is the liquid equilibrium concentration of dye in solution (mg/L), K_F (mg/g) and n_F are Freundlich constants for adsorption capacity and adsorption intensity respectively. A linear plot of ln qe versus ln Ce confirms the validity of the Freundlich model and the magnitude of 'n' indicates the favourability of the adsorption system; specifically, when the value of 'n_F' lies in $1 < n_F < 10$ range. Compared to the Freundlich model, the Langmuir model assumes a homogeneous adsorbent surface with identical sites which are equally distributed, energetically equivalent and each site carries equal number of molecules with no interaction between adsorbate molecules. The Langmuir adsorption isotherm model is not capable to explain the mechanism of adsorption process, but it provides information on adsorption capability and the equilibrium process behaviour as represented in the following expression:[69]

$$\frac{C_e}{q_e} = \frac{1}{(q_{max} \times K_L)} + \frac{C_e}{q_{max}} \qquad (10)$$

where q_e and Ce are defined as above, q_{max} and K_L represent the maximum adsorption capacity of the adsorbent and the energy constant related to the heat of adsorption respectively. In this study, the experimental data of the adsorption process of all the three samples was fit using the Langmuir and Freundlich isotherm models, the results of which are shown in Figure 16.

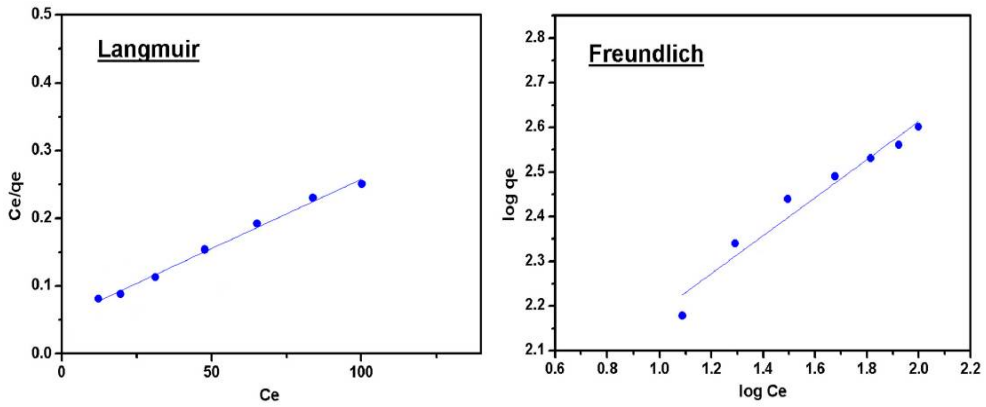


Figure 16. Adsorption isotherms for the adsorption of CVdye onto LDPE/5%MMT at 30 °C.

The adsorption parameters along with the correlation coefficients (R^2) are given in Table 5. The value of Freundlich constant 'n' lies between 1 and 10, indicating a favourable adsorption process of CV dye onto LDPE/5%MMT nanocomposite.

Table 5. Langmuir and Freundlich constants for the adsorption of CV dye (pH 6.2) onto LDPE/5%MMT nanocomposite at 30 °C (Dye conc. 50 – 200 mg L^{-1}).

Freundlich			Langmuir			
R2	Nf	Kf (mg/g)	R2	KL (L/mg)	qm (mg/g)	RL
0.935	2.1	94.019	0.9987	15.802	745.95	0.068-0.23

The higher correlation coefficient R^2 (>0.99) of the Langmuir equation suggest that the Langmuir equation can be used to fit the

experimental adsorption data and evaluate the maximum dye adsorption capacities of these adsorbents. Since, the Langmuir model assumes monolayer adsorption, the existence of homogenous active sites of the adsorbents could also be indicated. The highest maximum adsorption capacity of LDPE/5%MMT (746.27 $mg \cdot g^{-1}$) allows adsorption of more crystal violet dye molecules on its surface.

The reason behind very high adsorption capacity value of LDPE/MMT is the presence of variety of functional groups such as, –OH, –Si–O, –Al–O, –Fe–O and $–CH_2–CH_2–$ on the surface and edges of LDPE/MMT and their interactions (hydrogen bonding) with the dye which results in more and fast adsorption of cationic dyes.[70] Also, when compared to raw MMT, LDPE/5%MMT possesses a more extensive pore structure with higher BET specific surface area (242.14 $m^2 \cdot g^{-1}$) which further enhances the adsorption capacity of dye molecules.

Another important characteristic of Langmuir isotherm related to its shape is expressed in terms of a dimensionless constant, known as the equilibrium parameter (RL), using the following expression:

$$R_L = \frac{1}{1 + K_L C_0} \qquad (11)$$

where, K_L and C_0 are the Langmuir adsorption constant and the initial dye concentration, respectively. The value of R_L indicates four types of isotherms: (i) unfavourable ($R_L > 1$), (ii) linear ($R_L = 1$), (iii) favourable ($0 < R_L < 1$) and (iv) irreversible ($R_L = 0$).[71] In the present work, the calculated R_L values of the crystal violet dye adsorption are between 0 and 1, which further informs that the system follows favourable adsorption process (Table 5).

3.6. Adsorption thermodynamics

To investigate the effect of temperature on the adsorption of CV by the LDPE/5%MMT nanocomposite adsorbent, the adsorption process was studied at three different temperatures; 303 K, 313 K and 323 K.

According to results, the adsorption process is endothermic in nature, which indicates that the amount of adsorbed dye increases at higher temperatures. This enhancement of adsorption capacity of the nanocomposite at elevated temperatures may be attributed to the faster mobility followed by the increased penetration of the dye molecules inside the pores of LDPE/5%MMT at higher temperatures or the generation of new adsorption sites. It is known that a large proportion of the active sites of the MMT present in LDPE/5%MMT nanocomposite would be occupied by water molecules via hydrogen bonds. Therefore, increasing the temperature would result in the removal of water molecules, giving the space for the adsorption of dye molecules. Besides pore structure characteristics, the surface chemical characteristics are also important factors affecting the adsorption behaviour and provide useful information regarding the spontaneity of a system. To understand this, the values of thermodynamic parameters, such as change in free energy ($\Delta G°$), enthalpy ($\Delta H°$) and entropy ($\Delta S°$) were obtained by the following equations:

$$\Delta G° = -RT \ln K \quad (12)$$

$$K = \frac{q_e}{C_e} \quad (13)$$

$$\ln K = -\frac{\Delta G°}{RT} = -\frac{\Delta H°}{RT} + \frac{\Delta S°}{R} \quad (14)$$

$$\Delta G° = \Delta H° - T\Delta S° \quad (15)$$

where, K is the thermodynamic equilibrium constant, R (8.3145 $J \cdot mol^{-1} \cdot K^{-1}$) is the ideal gas constant, T (K) is the temperature during adsorption,

q_e is the adsorption capacity and C_e is the equilibrium concentration of CV. The values of change in enthalpy (ΔH°), and entropy change (ΔS°) can be obtained from the slope and intercept of ln K versus 1/T plot (Figure 17) using the Van't Hoff equation (Eq.11) while the (ΔG°) value were determined at various temperatures using Eq.9.

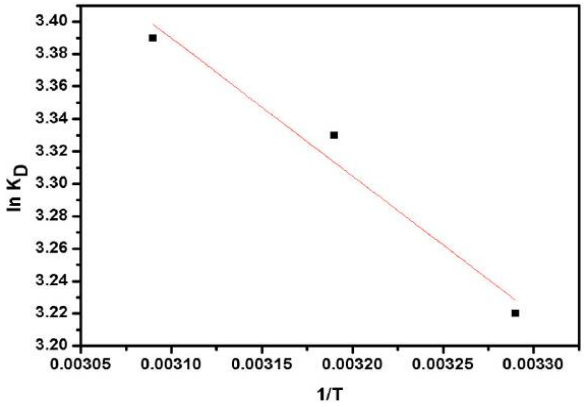


Figure 17. Van't Hoff plot for the adsorption of CV onto LDPE/5%MMT nanocomposite.

The overall negativity and the increase of ΔG° values with rising temperatures indicates a spontaneous and favourable adsorption process (Table 6), while the positive value of (ΔH°) depicts the endothermic nature of the adsorption process. Further, the positive value of the entropy change (ΔS°) suggests affinity of LDPE/5%MMT nanocomposite for CV dye and an increased randomness at the solid solution interface.

Table 6. Thermodynamic parameters for the adsorption of CV dye onto LDPE/5% MMT nanocomposite at different temperatures.

Temperature (K)	Parameters		
	ΔG° (kJ mol−1)	ΔH° (kJ mol−1)	ΔS° (J mol−1 K−1)
303	−8.11	-	-
313	−8.67	7.06	50.09
323	−9.11	-	-

3.7. Reusability test

To evaluate the reusability of the LDPE/5%MMT nanocomposite, the dye adsorbed nanocomposite particles were desorbed using ethanol solution, regenerated and then used for next adsorptive runs. It was observed that even after five cycles, there was a small decrease (~ 4.5%) in the CV dye removal efficiency of the LDPE/5%MMT nanocomposite as compared to the initial value. This change can be explained on the basis that the structure of some LDPE/5%MMT particles may have been slightly destroyed during the process of desorption, thereby inhibiting the adsorption of the CV molecules again. Furthermore, all of the dye molecules could not have been freed completely by desorption and some of them also may have remained in the interlayer spaces resulting in repulsive forces for the new dye molecules. The sample showed a fairly ideal adsorption capacity, illustrating good recycling potential and longevity of the nanocomposite (Figure 18). All the results demonstrate that these nanocomposite adsorbents can be applied in practical water treatment owing to their high adsorption capacity and good reusability.

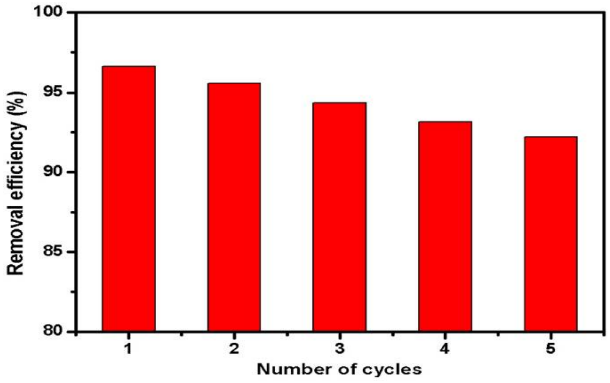


Figure 18. Reusability of the LDPE/5%MMT nanocomposite adsorbent.

Conclusion

Herein, LDPE/MMT nancomposites with different MMT nanoclay loadings were prepared successfully using melt extrusion. TEM confirmed

that MMT nanoclay was well dispersed in the LDPE matrix and exhibited exfoliation and partial intercalation. Owing to the formation of an insulating char layer during combustion, LDPE/MMT nanocomposites were found to be more thermally stable than pristine LDPE. The overall thermal stability was also found to increase with an increased content of MMT nanoclay. The results showed that the mid-point decomposition temperature ($T_{50\%}$) of the nanocomposite prepared with 10 wt % MMT is 497 ºC, which is a value that is 22 ºC higher than that of pristine LDPE (475 ºC). The tensile strength of this nanocomposite improved clearly by 40.87% in comparison to that of the pristine LDPE. A significant decrease in oxygen permeability (42.8%) and water vapor permeability (26.2%) with an increased MMT nanoclay content of up to 10 wt% was observed due to the tortuous structure across the LDPE matrix. The prepared nanocomposite (LDPE/5%MMT) was used for crystal violet dye adsorption and a very high adsorption capacity (746.27 $mg \cdot g^{-1}$) was achieved. The study also reveals a superior adsorption of CV dye on LDPE/5%MMT nanocomposite, indicating a significant positive role of MMT in the adsorption mechanism. The experimental data for the kinetics of the adsorption process supports pseudo-second-order kinetic model, suggesting that the adsorption rate depends upon the availability of the adsorption sites. The adsorption process was further investigated by Langmuir and Freundlich adsorption models wherein the equilibrium data fitted better to the Langmuir isotherm model with a negligible error, suggesting a homogeneous adsorption process to describe the dye-LDPE/5%MMT nanocomposite interaction. The adsorption is primarily an outcome of physical and electrostatic interactions owing to the existence of polar oxygen-containing functional groups like –OH, –Al–O, –Si–O, –Al–OH and –Fe–O. Moreover, the presence of aromatic non-functionalized

groups further facilitate the adherence of dye molecules through π-π interactions and hydrogen bonding on the surface of LDPE/5%MMT nanocomposite. In general, it can be concluded that the LDPE/5%MMT nanocomposite is a synergistically effective adsorbent and possesses a great potential in the removal of dyes from contaminated water.

Conflicts of interest

The authors have no competing interests to declare relevant to the content of this article.

References

1. Ononiwu, N. H.; Ozoegwu, C. G.; Madushele, N.; Akinlabi, E. T. Carbonization temperature and its effect on the mechanical properties, wear and corrosion resistance of aluminum reinforced with eggshell. *J. Compos. Sci.*, **2021**, *5*, 10. https://doi.org/10.3390/jcs5100262
2. Shabtai, I. A.; Lynch, L. M.; Mishael, Y.G. Designing clay-polymer nanocomposite sorbents for water treatment: A review and meta-analysis of the past decade. *Water Res.* **2021**, *188*, 116571. https://doi.org/10.1016/j.watres.2020.116571
3. Abulyazied, D. E.; Ene, A. An Investigative Study on the Progress of Nanoclay-Reinforced Polymers: Preparation, Properties and Applications: A Review. *Polymers* **2021**, *13(24)*, 4401. https://doi.org/10.3390/polym13244401
4. Boudjemaaa, S.; Djellouli, B. Characterization of organomont-morillonite (Organo-MMT) and study of its effects upon the formation of poly(methyl methacrylate)/Organo-MMT nanocomposites prepared by in-situ solution polymerisation. *Russ. J. Appl. Chem.*, **2015**, *87*, 1464 − 1473. https://doi.org/10.1134/S1070427214100127
5. Khader, E. H.; Muslim, S. A.; Saady, N. M.; Ali, N. S.; Salih, I. K.; Mohammed, Th. J.; Albayati, T. M.; Zendehboudi, S. Recent advances in photocatalytic advanced oxidation processes for organic compound degradation: a review. *Desalin. Water Treat.* **2024**, *318*, 100384. https://doi.org/10.1016/j.dwt.2024.100384
6. Kishor, R. D.; Purchase, G. D.; Saratale, R. G.; Saratale, L. F. R.; Ferreira, M.; Bilal, R.; Chandra, R.; Bharagava, N. Ecotoxicological and health

concerns of persistent coloring pollutants of textile industry wastewater and treatment approaches for environmental safety. *J. Environ. Chem. Eng.* **2021**, *9*, 105012. https://doi.org/10.1016/j.jece.2020.105012

7. Lisa, J. T.; Wei, Z.; Kun, Z. Recent progress on polymer materials for additive manufacturing. *Adv. Funct. Mater.* **2020**, *30(43)*, 2003062. https://doi.org/10.1002/adfm.202003062

8. Boudjemaa, S. Structural and thermal decomposition of organo montmorillonites (OMMT) studied by XRD, TGA and DSC: the role of surfactant agent concentration. *Rev. Roum. Chim.* **2019**, *64*(1), 35 – 44. https://doi.org/10.33224/rrch.2019.64.1.03

9. Al Rashid, Al Rashid, A.; Khan, S. A.; Al-Ghamdi, S. G.; Koç, M. Additive manufacturing of polymer nanocomposites: needs and challenges in materials, processes and applications. *J. Mater. Res. Technol.*, **2021**, *14*, 910 – 941. https://doi.org/10.1016/j.jmrt.2021.07.016

10. Althahban, S.; Alomari, A. S.; Sallam H. E.; Jazaa, Y. Preparation and characterization of snake plant fiber reinforced composite: A sustainable utilization of biowaste. *J. Mater. Res. Technol.* **2023**, *23*, 491 – 502. https://doi.org/10.1016/j.jmrt.2023.01.025

11. Mokhtar, A.; Abdelkrim, S.; Djelad, A.; Sardi, A.; Boukoussa, B.; Sassi M.; Bengueddach, A. Adsorption behavior of cationic and anionic dyes on magadiite-chitosan composite beads. *Carbohydr. Polym.* **2020**, *229*, 115399. https://doi.org/10.1016/j.carbpol.2019.115399

12. Kudva, A.; Gt, M.; Pai, K. D.; Jones, I. P. Mechanical, thermal, and morphological properties of low-density polyethylene nanocomposites reinforced with montmorillonite: Fabrication and characterizations. *Cogent. Eng*. **2022**, *9*(1), 2107770. https://doi.org/10. 1080/23311916.2022.2107770

13. Adeyemo, A. A.; Adeoye I. O.; Bello, O. S. Adsorption of dyes using different types of clay: A review. *Appl. Water Sc*i. **2017**, *7*, 543 – 568. https://doi.org/0.1007/s13201-015-0322-y

14. Khan, Z. I.; Habib, U.; Mohamad, Z. B.; Rahmat A. R. B.; N. Abdullah, A. S. B. Mechanical properties of wollastonite reinforced thermoplastic composites: A review. *Alexandria Eng. J*. **2022,** *61*(2), 975 – 990. https://doi.org/10. 1016/j.aej.2021.06.015

15. Hachemaoui, M.; Mokhtar, A.; Mekki, A.; Zaoui, F.; Abdelkrim, S.; Hacini, S.; Boukoussa, B. Preparation of activated carbon-reinforced composite beads based on MnO_2/MCM-41@Fe_3O_4 and calcium alginate for efficient removal of tetracycline in aqueous solutions. *Int. J. Biol. Macromol*. **2020**, *164*, 468 – 479. https://doi.org/10.1016/j.ijbiomac.2020.07.128

16. Holkar, C. R.; Jadhav, A. J.; Pinjari, D. V.; Mahamuni, N. M.; Pandit, A. B. A critical review on textile wastewater treatments: Possible approaches. *J. Environ. Manag*. **2016,** *182*(35), 1 – 66. https://doi.org/10.1016/j.jenvm an.2016.07.090

17. Shenouda, S. S.; Hussien, M. S. A.; Parditka, B.; Csik, A.; Takats V.; Erdelyi, Z. Photocatalytic crystalline and amorphous tio$_2$ nanotubes prepared by electrospinning and atomic layer deposition. *Ceram. Int.* **2020**, *46*, 7922 – 7929. https://doi.org/10.1016/j.ceram int.2019.12.012

18. Lovell, P. A.; Schork, F. J. Fundamentals of emulsion polymerization. *Biomacromolecules* **2020**, *21*(11), 4396 – 4441. https://doi.org/10.1021/acs.biomac.0c00769

19. Li, N.; Yang, B.; Xu, L.; Xu, G.; Sun W.; Yu, S. Photocatalytic crystalline and amorphous TiO_2 nanotubes prepared by electrospinning and atomic layer deposition. *Ceram. Int*. **2016**, *42*, 5979 – 5984. https://doi. org/10.1016/j. int.2015.12.145

20. Saadati, A.; Habibi-Yangjeh, A.; Khataee. A. Dual S-Scheme TiO2–x/BiOI/BiSI photocatalysts with boosted visible-light-activated efficiency for removal of contaminants. *Ind. Eng. Chem. Res*. **2025**, *64*(49), 23263 – 23276. https://doi.org/10.1021/acs.iecr.5c02869

21. Heibati, B.; Rodriguez-Couto, S.; Amrane, A.; Rafatullah, M.; Hawari, A.; Al-Ghouti, M. A. Adsorption of reactive Black-5 by pine needles biochar produced via catalytic and non-catalytic pyrolysis. *J. Ind. Eng. Chem*. **2014**, *20*, 2939 – 2947. https://doi.org/10.1016/j. jiec.2013.10. 063

22. Raj, S.; Singh, H. Treatment of textile industry wastewater based on coagulation-flocculation aided sedimentation followed by adsorption: Process studies in an industrial ecology concept. *J. Sci. Total Environ*. **2023**, *857*, 159464. https://doi.org/10.1016/j.scito tenv.2022.159464

23. Khemila, B.; Merzouk, B.; Chouder, A.; Zidelkhir, R.; Leclerc, J. Removal of a textile dye using photovoltaic electrocoagulation. *Sustain. Chem. Pharm*. **2018**, *7*, 27 – 35. https://doi.org/10.1016/j.scp.2017.11. 004

24. Xinghou, H.; Tianhan, K.; Ping, D. Heterojunction photocatalysts for degradation of the tetracycline antibiotic: a review. *Environ. Chem. Lett*. **2021**, *194*, 110499. https://doi.org/10.1016/j.envres.2020 110499

25. Ateia, M.; Alsbaiee, A.; Karanfil, T.; Dichtel, W. Efficient PFAS removal by amine-functionalized sorbents: critical review of the current literature. *Sci. Technol. Lett.* **2019**, *6*, 688 – 695. https://doi.org/10.1021/acs.estlett.9b00659

26. Ali, H.; Khan, E. What are heavy metals? Long-standing controversy over the scientific use of the term "Heavy Metals": proposal of a comprehensive definition. *Toxicol. Environ. Chem.* **2018**, *100*, 6 – 19. https://doi.org/10.1080/02772248.2017.1413652

27. Tabrizi, S.H.; Tanhaei, B.; Ayati, A.; Ranjbari, S. Substantial improvement in the adsorption behavior of montmorillonite toward Tartrazine through hexadecylamine impregnation. *Environ. Res.* **2022**, *204*, 111965. https://doi.org/10.1016/j.envres.2021.111965

28. Boudjemaa, S. Preparation and characterisation of montmorillonite-Fe^{3+} (MMT-Fe^{3+}) nanoclay mineral for crystal violet (CV) removal from aqueous solutions. *Rev. Roum. Chim*. **2020**, *65*(10), 943 – 953. https://doi.org/10.33224/rrch.2020.65.10.09

29. Chakraborty, A.; Ruzimuradov, O.; Gupta, R. K.; Cho J.; Prakash, J. TiO_2 nanoflower photocatalysts: Synthesis, modifications and applications in wastewater treatment for removal of emerging organic pollutants. *Environ. Res*. **2022**, *212*, 113550. https://doi.org/10. 1016/j.envres. 2022.113550

30. Ghaemi, N.; Madaeni, S.S.; Daraei, P.; Rajabi, H.; Shojaeimehr, T.; Rahimpour, F. Preparation, characterization and dyes wastewater treatmen. *J. Hazard Mater*., **2015**, *298*, 111 – 121. https://doi.org/10.1016/j. jhazmat.2015.05.018

31. Joshiba, G. J.; Kumar, P. S.; Rangasamy, G.; Ngueagni, P. T.; Pooja, G.; Balji, G. B. Iron doped activated carbon for effective removal of tartrazine and methylene blue dye from the aquatic systems: Kinetics, isotherms, thermodynamics and desorption studies. *Environ. Res*. **2022**, *215*, 114317. https://doi.org/10.1016/j.envres.2022.114317

32. Kameda, T.; Oba, J.; Yoshioka, T. New treatment method for boron in aqueous solutions using mg al layered double hydroxide: kinetics and equilibrium studies. *Hazard. Mater.* **2015**, *293*(1), 54 – 63. https://doi.org/10.1016/j.jhazmat.2015.03.015

33. Sameer, A. A. Mechanical and thermal characterisations of low-density polyethylene/nanoclay composites. *Polym. Polym. Compos.* **2021**, *29(8)*, 1325 – 1332. https://doi.org/10.1177/0967391120968441

34. Ullah, F.; Ji, G.; Irfan, M.; Gao, Y.; Shafiq, F.; Sun, Y. Adsorption performance and mechanism of cationic and anionic dyes by KOH activated biochar derived from medical waste pyrolysis. *Environ. Pollut.* **2022**, *314*, 120271. https://doi.org/10.1016/j.envpol. 2022.120271

35. Vazquez, A.; López, M.; Kortaberria, G.; Martín, L.; Mondragon, I. Modification of montmorillonite with cationic surfactants. Thermal and

chemical analysis including CEC determination. *Appl. Clay Sci.* **2008**, *41*, 24 – 36. https://doi. org/10.1016/j.clay.2007.10.001

36. Tee, G. T.; Gok, X. Y.; Yong, W. F. Adsorption of pollutants in wastewater via biosorbents, nanoparticles and magnetic biosorbents: A review. *Environ. Res*. **2022**, *212*, 113248. https://doi. org/10.1016/j.envres.2022.113248

37. Marzbani, T.; Khayatian, Gh. Application of magnesium oxide nanoparticles for sunset yellow removal in aqueous solutions: adsorption isotherm, kinetic, and thermodynamic studies. *Iran. J. Chem. Chem. Eng.* **2022**, *41*(12), 4015 – 4025. https://doi.org/10.30492/ijcce.2022.529057.4696

38. Mallakpour, S.; Hatami, M. Magnetic magnetite-graphene oxide (Fe_3O_4-GO) nanocomposites for removal of dyes from aqueous solution. *Appl. Clay Sci.* **2019**, *174*, 127 – 137. https://doi.org/10.1016/j.clay.2019.03.026

39. Yu, J.; Wang, Q.; O'Har, D.; Sun, L. Preparation of two dimensional layered double hydroxide nanosheets and their applications. *Chem. Soc. Rev.* **2017**, *46*(19), 5950 – 5974. https://doi.org/10.1039/C7CS00318H

40. Zbik M. S.; Frost, R. L. Transmission X-ray Microscopy (TXM) Reveals the Nanostructure of a Smectite Gel. *J. Colloid Interface Sci.* **2010**, *346*, 311 – 316. https://doi.org/10.1016/j.jcis.2010.02.018

41. Merinska, D.; Kubisova, H.; Kalendova, A.; Svoboda, P. Processing and properties of polyethylene/montmorillonite nanocomposites. *J. Thermoplast. Compos. Mater.* **2012**, *25(1)*, 115 – 131. https://doi.org/10.1177/0892705711404939

42. Panwar, A.; Choudhary, V.; Sharma, D. K. Stability of organically modified montmorillonites and their polystyrene nanocomposites after prolonged thermal treatment. *J. Reinf. Plast. Compos.* **2011**, *30*, 446 – 459. https://doi.org/10.1177/0731684411399132

43. Kim, S. G.; Lofgren E. A.; Jabarin, S. A. The effect of particle size distribution on the dispersion of nanoclays in poly(ethylene terephthalate)/clay nanocomposites. *J. Appl. Polym. Sci.* **2013**, *127*, 2201 – 2212. https://doi.org/10.1002/app.37796

44. Abbasian, M.; Pakzad, M.; Amirmanesh, M. Modification of high-density polyethylene through the grafting of methyl methacrylate using RAFT Technique and Preparation of Its Polymer/Clay Nanocomposites. *Polym. Compos*. **2017**, *38*, 1127–1134. https://doi.org/10.1177/0095244318799498

45. Hussein, M.A.; Abdelaal, M.Y. An overview on polysulphone/clay nanocomposites. *Int. J. Biosen. Bioelectron.* **2017**, *3*(1), 201 – 205. https://doi.org/10.15406/ijbsbe.2017.03.00049

46. Zhang, Y.; Xu, H.; Lu, S. Preparation and application of layered double hydroxide nanosheets, *RSC Adv.* **2021**, *11*(39), 24254.

https://doi.org/10.1039/D1RA03289E

47. Delogu, F.; Gorrasi, G.; Sorrentino, A. Fabrication of polymer nanocomposites via ball milling: Present status and future perspectives. *Prog. Mater. Sci.* **2017**, *86*, 75 – 126. https://doi.org/10.1016/j.pmatsci.2017.01.003

48. Bhattacharya, M. Polymer nanocomposites - a comparison between carbon nanotubes, graphene, and clay as nanofillers. *Materials* **2016**, *9*(4), 262. https://doi.org/10.3390/ma9040262

49. Hu, K.; Kulkarni, D. D.; Choi, I.; Tsukruk, V. V. The overlooked role of reduced graphene oxide in the reinforcement of hydrophilic polymers. *Prog. Polym. Sci.* **2014**, *39*, 1934 – 1972. https://doi.org/10.1016/j.progpolymsci.2014.03.001

50. Jayrajsinh, S.; Shankar, G.; Agrawal Y. K.; Bakre, L. Montmorillonite nanoclay as a multifaceted drug-delivery carrier: A review. *J. Drug Deliv. Sci. Technol*. **2017**, *39*, 200 – 209. https://doi.org/10.1016/j.jddst.2017.03.023

51. Almasri, D. A.; Essehli, R.; Tonga, Y.; Jenny, L. Layered Zinc Hydroxide as an Adsorbent for Phosphate Removal and Recovery from Wastewater. *RSC Adv.* **2021**, *11*(48), 30172–30182. https://doi.org/10.1039/D1RA04279C

52. Azzam, W. R. Behavior of modified clay microstructure using polymer nanocomposites technique. *Alex. Eng. J.* **2014**, *53*(1), 143 – 150. https://doi.org/10.1016/j.aej.2013.11.010

53. Kotal M.; Bhowmick, A.K. Polymer nanocomposites from modified clays: Recent advances and challenges. *Prog. Polym. Sci.* **2015**, *51*, 127 – 187. https://doi.org/10.1016/j.progpolymsci.2015.10.001

54. Bitinis, N.; Hernandez, M.; Verdejo, R.; Kenny, J. M.; Lopez-Manchado, M. A. Polyamide/Polypropylene/graphene oxide nanocomposites with functional compatibilizers: Morpho-structural and physico-mechanical characterization. *Adv. Mater*. **2011**, *23*, 5229 –5 236. https://doi.org/10.1002/adma.201101948

55. Tu, W.; Zhou Y.; Zou, Z. Versatile Graphene-Promoting Photocatalytic Performance of Semiconductors: Basic Principles, Synthesis, Solar Energy Conversion, and Environmental Applications. *Adv. Funct. Mater*. **2013**, *23*, 4996 – 5008. https://doi.org/10.1002/adfm.201203547

56. Aoyama, S.; Ismail, I.; Park, Y. T.; Yoshida, Y.; Macosko, C. W.; Ougizawa, T. Polyethylene Terephthalate / Trimellitic Anhydride Modified Graphene Nanocomposites. *ACS Appl. Nano Mater.* **2018**, *1*(11), 2077–2085. https://doi.org/10.1021/acsanm.8b01525

57. Fu, J.; Naguib, H. E.; Effect of nanoclay on the mechanical properties of PMMA/clay nanocomposite foams. *J. Cell. Plast.* **2006**, *42*, 325 – 342. https://doi.org/10.1177/0021955X06063517

58. May, P.; Khan, U.; O'Neill A.; Coleman, J. N. Approaching the theoretical limit for reinforcing polymers with grapheme. *J. Mater. Chem*. **2012**, *22*, 1278 – 1282. https://doi.org/10.1039/C1JM15467B

59. Ahsani-Namin, Z.; Norouzbeigi R.; Shayesteh, H. Green mediated combustion synthesis of copper zinc oxide using Eryngium planum leaf extract as a natural green fuel: Excellent adsorption capacity towards Congo red dye. *Ceram. Int.* **2022**, *48*, 20961 – 20973. https:// doi.org/10.1016/j.ceram int.2022.04.090

60. Kiranşan, M.; C. Soltani, R.D.; Hassani, A.; Karaca S.; Khataee, A. Study of equilibrium and kinetic adsorption of rhodamine B onto purified bentonite clays. *J. Taiwan Inst. Chem. Eng*. **2014**, *45*, 2565 – 2577. https://doi.org/10.1016/j.jtice.2014.06.007

61. Yuh-Shan, H. Citation review of Lagergren kinetic rate equation on adsorption reactions. *Scientometrics* **2004**, *59*, 171 – 177. https://doi.org/10.1023/B:SCIE.*0000013305.99473.cf*

62. Shahwan, T.; Environ J. Sorption kinetics: obtaining a pseudo-second order rate equation based on a mass balance approach. *Chem. Eng*. **2014**, *2*, 1001 – 1006. https://doi.org/10.1016/j.jece.2014.03.020

63. Chen H.; Wang, A. Kinetic and isothermal studies of lead ion adsorption onto palygorskite clay. *J. Colloid Interface Sci*. **2007**, *307*, 309 – 316. https://doi.org/10.1016/j.jcis.2006.10.054

64. Tekin, N.; Şafaklı A.; Bingöl, D. Process modeling and thermodynamics and kinetics evaluation of Basic Yellow 28 adsorption onto sepiolite. *Desalin. Water Treat.* **2015**, *54*, 2023 – 2035. https://doi.org/10.1080/19443994.2014.893843

65. Sharma, P.; Borah, D. J.; Das P.; Das, M. R. Cationic and anionic dye removal from aqueous solution using montmorillonite clay: evaluation of adsorption parameters and mechanism. *Desalin. Water Treat.* **2016**, *57*, 8372 – 8388. https://doi.org/10.1080/19443994.2015.1021844

66. Boudjemaa S.; Zidelkheir, B. Removal properties of methylene blue from aqueous solutions by organomodified montmorillonite: isotherm, thermodynamics and kinetic studies. *Rev. Roum. Chim*. **2020**, *65*(5), 499 – 508. https://doi.org/10.33224/rrch.2020.65.5.10

67. Fan, L.; Luo, C.; Sun M.; Qiu, H. Synthesis of graphene oxide decorated with magnetic cyclodextrin for fast chromium removal. *J. Mater. Chem*. **2012**, *22*, 24577. https://doi.org/10.1039/c2jm35378d

68. Freundlich, H. On Adsorption in Solutions, *Für Phys. Chem*. **1907**, *57U*. https://doi.org/10.1515/zpch-1907-5723

69. Langmuir, I. The Constitution and Fundamental Properties of Solids and Liquids. Part I. Solids. *J. Am. Chem. Soc*. ***1916***, *38*, 2221 – 2295. https://doi.org/10.1021/ja02268a002

70. Altenor, S.; Carene, B.; Emmanuel, E.; Lambert, J.; Ehrhardt J. J.; Gaspard, S. Adsorption of methylene blue onto activated carbon produced from tea (Camellia sinensis L.) seed shells: kinetics, equilibrium, and thermodynamics studies. *J. Hazard. Mater*. **2009**, *165*, 1029 – 1039. https://doi.org/10.1016/j.jhazmat.2008.10.133

71. Mahmoodi, N. M.; Hayati, B.; Arami M.; Lan, C. Adsorption of textile dyes on Pine Cone from colored wastewater: Kinetic, equilibrium and thermodynamic studies. *Desalination* **2011**, *268*, 117 – 125. https://doi.org/10.1016/j.desal.2010.10.007